Journal of The Electrochemical Society, **161** (3) A355-A363 (2014)
0013-4651/2014/161(3)/A355/9/$31.00 © The Electrochemical Society

A Li-Rich Layered Cathode Material with Enhanced Structural Stability and Rate Capability for Li-on Batteries

Mehmet Nurullah Ates,[a,b,*] Sanjeev Mukerjee,[a,] and K. M. Abraham[a,b,**,z]**

[a]*Center for Renewable Energy Technology, Department of Chemistry and Chemical Biology, Northeastern University, Boston, Massachusetts 02115, USA*
[b]*NSF Center for High-Rate Nanomanufacturing, Northeastern University, Boston, Massachusetts 02115, USA*

A new lithium rich composite positive electrode material of the composition $0.3Li_2MnO_3.0.7LiNi_{0.5}Co_{0.5}O_2$ (LLNC) was synthesized using the conventional co-precipitation method. Its crystal structure and electrochemistry in Li cells have been compared to that of the previously known material, $0.3Li_2MnO_3.0.7LiMn_{0.33}Ni_{0.33}Co_{0.33}O_2$ (LLNMC). The removal of Mn from the $LiMO_2$ (M = transition metal) segment of the composite cathode material allowed us to determine the location of the manganese oxide moiety in its structure that triggers the layered to spinel conversion during cycling. The new material resists the layered to spinel structural transformation under conditions in which LLNMC does. X-ray diffraction patterns revealed that both compounds, synthesized as approximately 300 nm crystals, have identical super lattice ordering attributed to Li_2MnO_3 existence. Using X-ray absorption spectroscopy we elucidated the oxidation states of the K edges of Ni and Mn in the two materials with respect to different charge and discharge states. The XAS data along with electrochemical results revealed that Mn atoms are not present in the $LiMO_2$ structural segment of LLNC. Electrochemical cycling data from Li cells further revealed that the absence of Mn in the $LiMO_2$ segment significantly improves the rate capabilities of LLNC with good capacity maintenance during long term cycling. Removing the Mn from the $LiMO_2$ segment of lithium rich layered metal oxides appears to be a good strategy for improving the structural robustness and rate capabilities of these high capacity cathode materials for Li-ion batteries.
 [DOI: 10.1149/2.070403jes]

Manuscript submitted November 27, 2013; revised manuscript received December 20, 2013. Published January 3, 2014.

The lithium rich layered metal oxide cathode materials of the formula $(1–x)Li_2MnO_3.xLiMnO_2$ for Li-ion batteries have spurred great interest due to their exceptionally high discharge capacities, reaching almost 300 mAh/g,[1,2] or one electron transfer per transition metal. These materials, also known as layered metal oxide composite cathodes, offer the greatest promise to meet the energy and power demands of batteries for hybrid electric vehicles (HEVs) and electric vehicles (EVs). The myriad investigations reported to further advance these cathode materials include substitution of some of the Mn in the $LiMnO_2$ segment of parent structure with other transition metals,[3–6] special surface treatments using $(NH_4)_2HPO_4$ solution[7] and ZnO,[8] and coating with the Li^+-conducting solid electrolyte LiPON[9] aiming to improve the surface chemistry of $(1–x)Li_2MnO_3.xLiMnO_2$ during Li_2O removal. Other modifications of these composite cathode materials attempted include suppression of possible oxygen vacancies created during Li_2MnO_3 activation and development of new preparation methods. Among the alternative syntheses methods, there is a microsphere particle driven method,[10] molten salt technique,[11] and synthesis directly from Li_2MnO_3 to incorporate NiO rock-salt regions[12] to enhance rate capability. During the first charge of $(1–x)Li_2MnO_3.xLiMO_2$, (where M = Mn, Ni and Co) Li extraction from the $LiMO_2$ segment occurs between 3.5 and 4.3 V, followed by the extraction of Li_2O (as Li^+ and O_2) from the Li_2MnO_3 portion, along with some electrolyte decomposition, at potentials between 4.3 and 5 V. The first charging process of these classes of materials is vital as it establishes the structural integrity between the Li_2MnO_3 and $LiMO_2$ segments in the composite oxide. In spite of aforementioned improvement efforts, some significant drawbacks of these materials still remain to be resolved. They include: i-) the irreversible capacity loss (ICL) in the first charge accompanied by oxygen evolution,[13] ii-) transformation from layered to spinel structures during long-term cycling, especially at slightly elevated temperatures,[14] and iii-) low rate capability, ascribed in part to the low conductivity of these materials.[15]

In this paper, we report the synthesis and characterization of a layered composite positive electrode material of the formula $0.3Li_2MnO_3.0.7LiNi_{0.5}Co_{0.5}O_2$ (abbreviated LLNC) and compare its performance to the previously known $0.3Li_2MnO_3 0.7LiMn_{0.33}Ni_{0.33}Co_{0.33}O_2$ (called LLNMC). A major difference between the two materials is that Mn is absent in the $LiMO_2$ layer segment of the new composite cathode material. We have found that removing Mn from the structure in this fashion has improved the material in several ways. The LLNC positive electrode material has higher rate capability, resists the layer to spinel structural conversion during cycling, and is stable with respect to charge to 5 V. The present study has also provided information on how the absence of Mn in the $LiMO_2$ segment of the composite cathode structure affects its rate capability and the layered to spinel structural transformation.

The new cathode material, $0.3Li_2MnO_3 0.7LiNi_{0.5}Co_{0.5}O_2$, has been thoroughly characterized by means of X-ray diffraction (XRD), field emission scanning electron microscopy (FESEM) combined with energy-dispersive X-ray spectroscopy (EDS) analysis, and X-ray absorption spectroscopy (XAS). The discharge/charge capacities and cycling behavior of LLNC was examined at room temperature and 50°C to elucidate its rate capability and structural stability, in particular its susceptibility to transform from the layered to the spinel phase. X-ray absorption spectroscopy (XAS) was used to identify the oxidation states of Mn and Ni atoms at various stages during the initial charge and discharge. Our results show that the location of the Mn atom determines the robustness of the composite oxide structure and influences its rate capability.

The two materials LLNC and LLNMC can be represented alternatively as, $Li[Li_{0.130}Mn_{0.261}Ni_{0.304}Co_{0.304}]O_2$ and $Li[Li_{0.130}Mn_{0.463}Ni_{0.203}Co_{0.203}]O_2$, respectively. However, these representations do not identify the two types of Mn present in the structures. As a result the composite formulation is used throughout this paper since as shown below the two materials exhibit markedly different phase transition behavior during cycling at 50°C.

Experimental

The materials having the composition of $0.3Li_2MnO_3 0.7LiMn_{0.33}Ni_{0.33}Co_{0.33}O_2$ and $0.3Li_2MnO_3 0.7LiNi_{0.5}Co_{0.5}O_2$, denoted as LLNMC and LLNC, respectively, were synthesized using conventional co-precipitation method. In this procedure nitrate salts of manganese, nickel and cobalt, [$(Mn(NO_3)_2.4H_2O$, $Ni(NO_3)_2.6H_2O$, and $Co(NO_3)_2.6H_2O$)], were dissolved in water followed by co-precipitation of mixed metal hydroxides under a mildly alkaline condition. The PH of solution was maintained at 11–12 (as monitored by SympHony pH meter, model SP70P). The precipitated mixture of metal hydroxides were filtered and washed in copious deionized water at least twice making sure possible impurities like $LiNO_3$ were removed. The precipitate was dried in a vacuum oven and then intimately

*Electrochemical Society Student Member.
**Electrochemical Society Fellow.
zE-mail: kmabraham@comcast.net

mixed with an appropriate amount of $LiOH.H_2O$ and pelletized. The powders were then heat-treated in atmospheric air for: i) 3 hours at 480°C, followed by pelletizing the powders and then ii) heating for 3 hours at 900°C. A 3 wt% excess of $LiOH.H_2O$ was used to compensate for possible lithium evaporation loss during the sintering.

To prepare a Ni^{4+} reference material for XAS experiments, $LiNi_{0.85}Co_{0.15}O_2$ was synthesized via solid state reaction from appropriate amounts of $LiOH.H_2O$, $Ni(Ac)_2.4H_2O$ and $Co(Ac)_2.4H_2O$. The precursor mixture was thoroughly mixed and fired at 630°C for 8 hours and the powder was ground, pelletized and fired at 750°C for another 16 hours. Charging of this material in a Li cell to 5.1 V produced the Ni^{4+} reference material.[16]

X-ray diffraction spectra were recorded over the 2θ range of 10–80 degrees with a Rigaku Ultima IV diffractometer using CuKα radiation. Unit cell constants of the synthesized compounds were refined with PDXL software program provided by Rigaku Corporation. XRD unit cell visualizations were run via VESTA software.[17] Particle morphology measurement and elemental analysis were performed with a Hitachi S-4800 Field emission scanning electron microscope (FESEM) combined with its energy dispersive X-ray spectroscopy (EDAX) attachment.

Galvanostatic charge/discharge cycling was performed on an Arbin Instruments BT2000 model cycler. Pressed cathode electrodes were prepared from 80 weight percent (w/o) active material, 10 w/o Super-P conductive carbon (TimCal), and 10 w/o polyvinylideneflouride (PVDF). The electrode mix slurry made with N-methyl-2- pyrrolidone (NMP) was cast on an aluminum foil (with doctor blade to control thickness) and dried overnight at 100°C under vacuum. The electrodes had typical active material loading of at least 4–5 mg/cm^2. Coin cells were assembled in an argon-filled glove box and filled with 1 M $LiPF_6$ /1:1.2 EC/DMC electrolyte. A porous polypropylene membrane separated the active positive electrode and lithium foil negative electrode in the cell. The cells were cycled at room temperature and 50°C. The theoretical capacity of both composite compounds were taken as 280 mAh/g. Room temperature cyclic voltammetry measurements were performed in the range of 2–4.9 V with a 50 μV/s scan rate on a Voltalab PGZ402 model instrument.

X-ray absorption spectroscopy measurements were performed in the transmission mode at the Ni and Mn-K edges at beam line X-3A of the National Synchrotron Light Source at Brookhaven National Laboratory. Electrodes from cells cycled at low rates (C/20) were extracted and sealed in Kapton tape and then stored in glass vials taped with Teflon tape and packed in moisture impermeable aluminized bags under argon to avoid any possible oxidation during transportation to the Light source. The data were processed and fitted using the Athena and Artemis software programs. Scans were calibrated, aligned and normalized with background removed using the IFEFFIT suite.[18,19]

Results and Discussion

The layered to spinel structural transformation during cycling of lithium rich composite cathodes of the type $xLi_2MnO_3(1-x)LiMn_{0.33}Ni_{0.33}Co_{0.33}O_2$ has been investigated by several groups.[13,14,20,21] However, the cause for this problem is not fully understood especially with respect to the specific transition metal that causes the structural conversion. Thackeray et al suggested that the layered to spinel conversion was triggered by the Li_2MnO_3 segment of the integrated lithium rich composite oxide. They also pointed out this specific spinel growth may stabilize the oxide structure. Aurbach and his group[21] claimed, based on micro-beam electron diffraction patterns, that the conversion took place even before

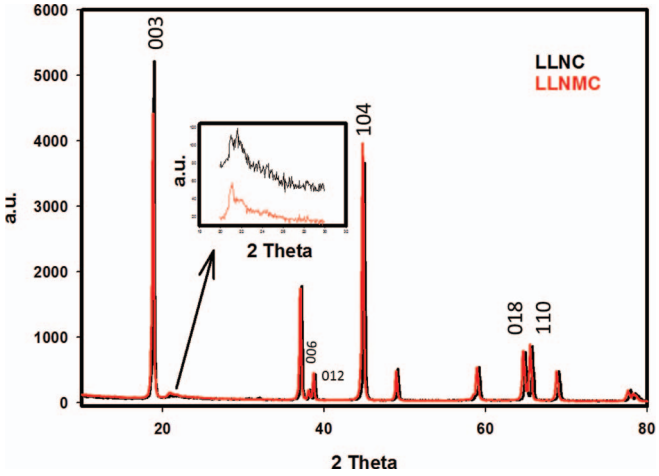

Figure 1. XRD patterns of both LLNMC (red) and LLNC (black) pristine powders.

the activation of Li_2MnO_3 which advocates that the cause of such conversion is the $LiMO_2$ segment of the integrated structure. Their findings were supported by other groups as well.[22] To shed further light on this point, we synthesized $0.3Li_2MnO_3 0.7LiNi_{0.5}Co_{0.5}O_2$ that does not contain Mn in the $LiMO_2$ segment. This has allowed us to show here that Mn present in the $LiMO_2$ segment of the composite triggers the layered to spinel conversion. We have found the new material LLNC composite without Mn in its $LiMO_2$ segment to maintain its crystal structure under long term cycling at 50°C when $0.3Li_2MnO_3 0.7LiMn_{0.33}Ni_{0.33}Co_{0.33}O_2$ cycled at identical conditions is converted to the spinel structure.

Composition and structure of LLNC.— Figure 1 shows the XRD patterns of LLNMC (red) and LLNC (black) metal oxides. Both materials exhibit similar patterns suggesting that they possess similar crystal structures. All of the diffraction peaks can be indexed to a pseudo-trigonal unit cell with *R3m* symmetry. Specifically, the weak diffraction peaks at 2θ values between 21° and 25° are characteristic of the Li_2MnO_3 crystalline component in the integrated composite cathode structure as noted by others.[23,24] The inset in Figure 1 indicates that both compounds have similar amount of the Li_2MnO_3 segment. Moreover, the (006)/(012) and (018)/(110) doublets clearly indicate a highly ordered layered structure for both of the composite materials.[11] The ratio of the intensities of the two major peaks I(003)/I(104) is a direct indication of cation mixing.[25,5] Table I displays the unit cell parameters along with the ratio of I(003)/I(104). As can be seen from the data, the ratio of I(003)/I(104) for LLNC has higher value than that of LLNMC which supports the view that LLNC has effectively suppressed cation mixing. It is believed that cation mixing takes place during sintering when Ni^{2+} enters the Li^+ site causing small crystal distortions.[26,27] Less cation mixing in LLNC is plausible since Ni atoms appear to be in the 3^+ valance state as found with XAS discussed later. From Table I, one can also surmise that LLNC has smaller unit volume and 'a' parameter than LLNMC. This can be ascribed to the fact that Ni^{3+} in LLNC has smaller ionic radius (0.56 Å) than Ni^{2+} (0.69 Å) believed to be present in LLNMC (see EXAFS data later). By using the relative intensity ratio (RIR) technique, we determined the fraction of each layered segment (Li_2MnO_3 and $LiMO_2$) in each of the integrated composite cathode. It was around 78% of

Table I. Refined crystal parameters of pristine LLNMC and LLNC powders. Targeted space group selected was R3m.

Compound	a(A)	c(A)	V(A^3)	c/a	I(003)/I(104)	Refinement Parameters	Fraction of Li2MnO3/LiMO2(%)
LLNMC	2.8411	14.1660	99.026	4.9861	1.114	Rwp:13.56, Rp:9.28, Re:7.41, S:1.83	22/78 ($LiMn_{0.33}Ni_{0.33}Co_{0.33}O_2$=$LiMO_2$)
LLNC	2.8399	14.1665	98.946	4.9884	1.426	Rwp:10.84, Rp:8.79, Re:4.27, S:2.54	29/71 ($LiNi_{0.5}Co_{0.5}O_2$=$LiMO_2$)

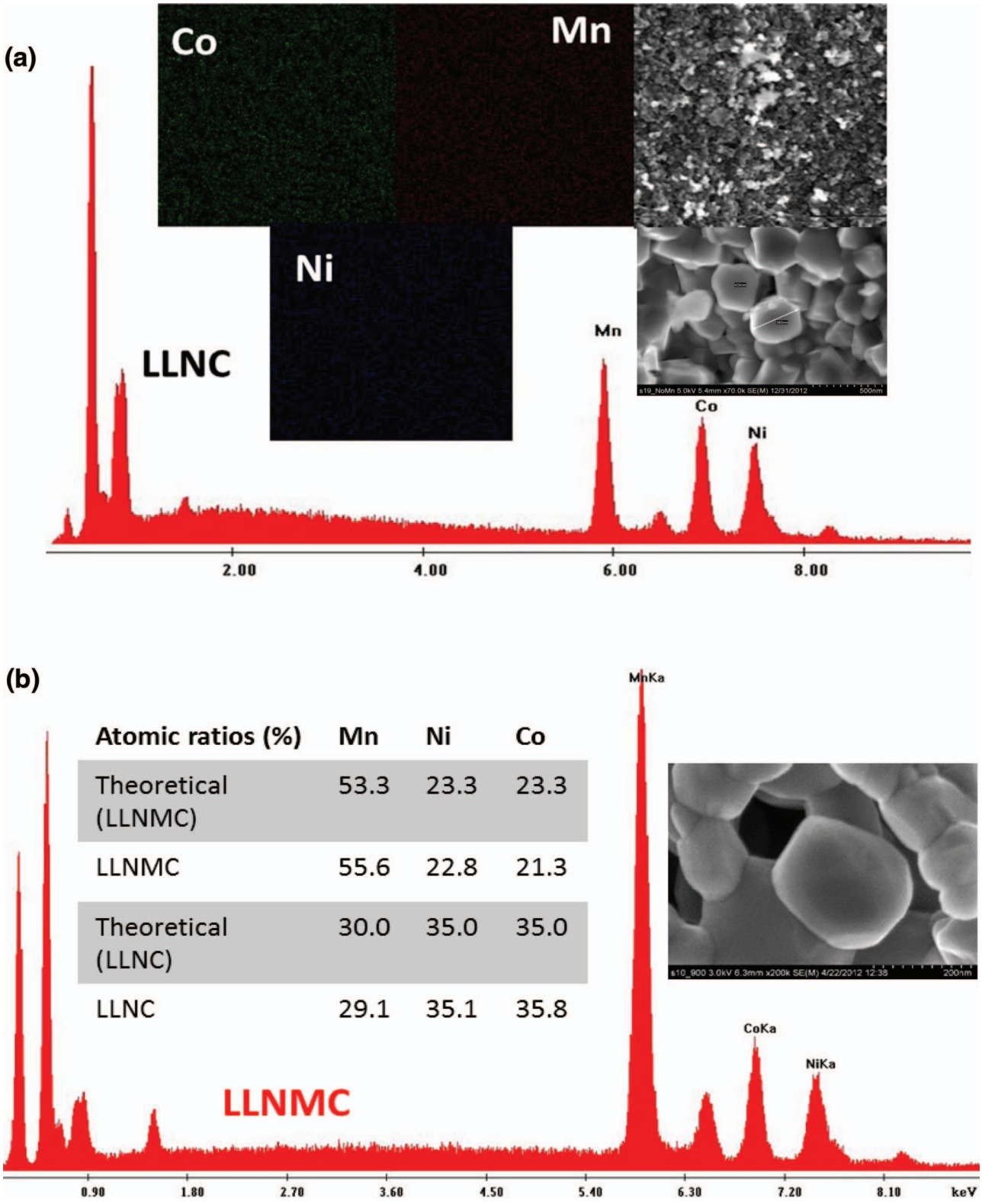

Figure 2. EDAX profiles, mapping figures and metal contents of the materials along with an FESEM; Figure a-) LLNC b-) LLNMC

$LiMn_{0.33}Ni_{0.33}Co_{0.33}O_2$ and 22 of Li_2MnO_3 in LLNMC and 71% of $LiNi_{0.5}Co_{0.5}O_2$ and 29% of Li_2MnO_3 in LLNC (Table I). The atomic coordinates for both phases were not further refined as well as stacking faults; however; the fraction values obtained is in the range of acceptable accuracy as reported in a study elsewhere used with similar technique.[28]

A morphological investigation using FESEM attests to the nanometer size particles of both active materials as displayed in Figure 2a and 2b. Both LLNMC and LLNC powders revealed similar particle sizes and transition metal contents based on the EDAX profiles presented in Figure 2a and 2b. The table displayed in the inset of Figure 2b shows theoretical and experimental metal contents for each

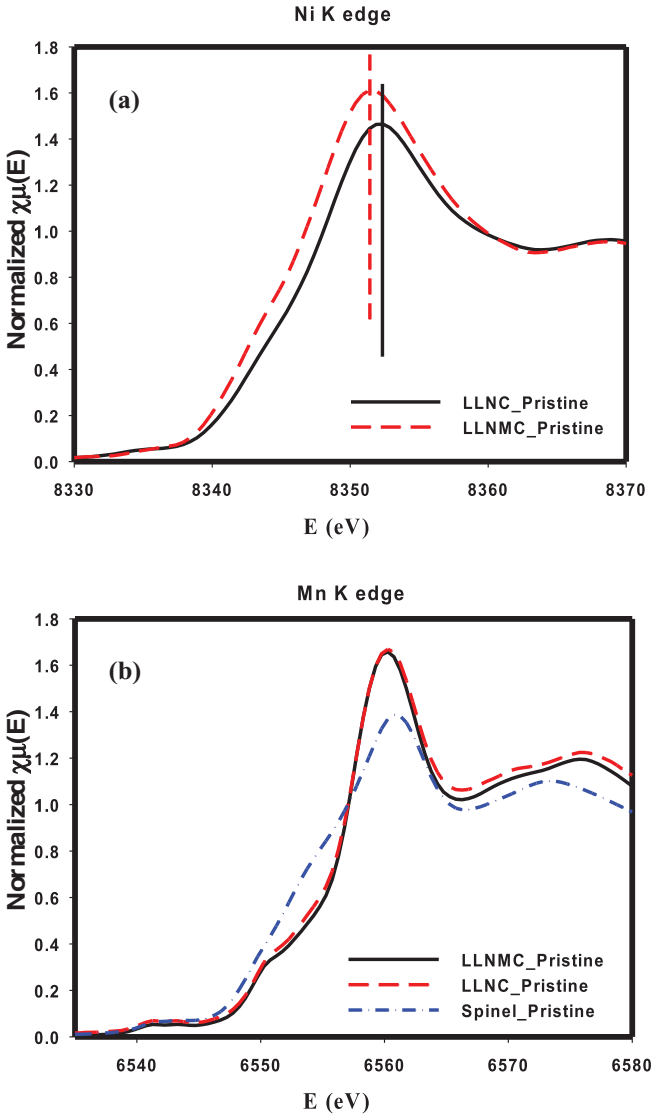

Figure 3. a-) Ni K-Edge XANES data; b-) Mn K-Edge data for LLNMC and LLNC pristine materials along with spinel reference.

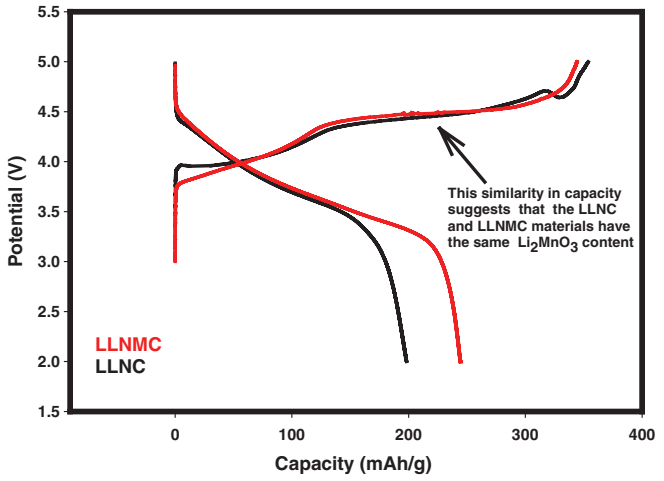

Figure 4. First cycling behavior of LLNC (black) and LLNMC (red) at room temperature between 2 – 4.9 V at C/20 rate.

compounds. We note that although EDAX technique is not a rigid way to determine the elemental composition; the data represent the average of many samples with runs on several segments of each sample, thereby providing an unambiguous measure of elemental composition of each material. The elemental mapping done with the FESEM also revealed a homogenous distribution of transition metals over the sample surface as depicted in, Figure 2a for LLNC.

In order to identify whether all of the Mn atoms are located in the Li_2MnO_3 segment of the composite structure or not, we performed XAS analysis for the pristine compounds. One should keep in mind that, determining average Mn oxidation states via XAS have been an issue as noted by others.[29] Therefore, our initial focus was on the Ni-K edge of the pristine materials. Since Ni exists in only the $LiMO_2$ portion of the oxide and the valance state of Co is 3^+ for both composite materials, the valance state of Ni solely influenced by the existence of Mn atoms. Figure 3a displays Ni-K edge XANES profiles for both LLNMC and LLNC pristine powders. The shift to higher energy values for LLNC compared to LLNMC supports the view that Ni has higher valence state due to removal of Mn from the $LiMO_2$ segment. This augurs well with our view that $LiMO_2$ portion of the LLNC does not host Mn atoms. Overall, we can approximate that during cycling Ni^{2+}/Ni^{4+} and Ni^{3+}/Ni^{4+} redox couples are active for LLNMC and LLNC, respectively. This will be discussed in detail in a later section. We also performed Mn-K edge for the same pristine materials and the normalized XANES profile pertaining to this experiment is shown in Figure 3b. The average oxidation states of Mn atoms are similar to each other which is not surprising since in both locations, Mn atoms have 3.44 valance state as stated by Thackeray et al.[20] This supports our observation that both materials in the pristine state have very little shift to lower energy values with respect to the spinel ($Mn^{3.5+}$) reference material as shown in Figure 3b.

The question arises as to why there is no Mn in the $LiMO_2$ segment of the LLNC composite when considering that both LLNC and LLNMC are prepared by the same method. Previous first principle calculations as well as Li MAS NMR spectroscopy studies showed that if excess Li was incorporated into layered metal oxide cathode materials in which Mn^{4+} existed along with Ni^{2+} and Co^{3+}, Li would preferentially be surrounded first by six Mn atoms,[23,30] instead of Ni and Co,[20] to create an intergrowth of Li_2MnO_3 phase to form the LLNMC composite structure. This behavior can be understood from a consideration of the ionic radii of these metals with Mn^{4+} (0.54A) having smaller ionic radius than Ni^{2+} (0.70A) and Co^{3+} (0.61A). Overall, Ni and Co prefers to occupy larger sites while Mn prefers smaller sites as in the layers of Li_2MnO_3. In the preparation of LLNC in which the amount of Mn^{4+} is relatively small, the Li_2MnO_3 phase is preferentially formed first with little Mn^{4+} left to occupy the $LiMO_2$ layer, whereas in LLNMC, there is sufficient amount of Mn^{4+} available to form the minimum content of Li_2MnO_3 first and then fill the $LiMO_2$ layers. It appears that in the preparation of Li rich layered composite metal oxide materials, there is a minimum $LiMn_2O_3$ content first formed in the composite structure before distributing any Mn^{4+} into the $LiMO_2$ layers to produce higher capacity materials like LLNMC. These considerations complemented by XRD, XAS, CV and first charge-discharge profiles support that in our LLNC compound little or no Mn exists in the $LiMO_2$ layer segment of the composite. Our investigations of a series of LLNMC compositions with various Li_2MnO_3 and $LiMO_2$ ratios suggest that when the ratio of Mn to (Co+Ni) is $<$ 03/0.7, all of the Mn is converted to Li_2MnO_3 to form LLNC.

Electrochemistry in lithium cells.— The first charge/discharge profiles are displayed in Figure 4 for LLNC (black) and LLNMC (red). Both compounds reached similar charging capacity with a single sloping and plateau regions indicating that each material possesses the integrated layered-layered structures. The LLNMC cathode delivers approximately 240 mAh/g discharge capacity at the C/20 rate, while LLNC exhibits around 200 mAh/g discharge capacity at the same rate. The reason why LLNC has lower first discharge capacity than

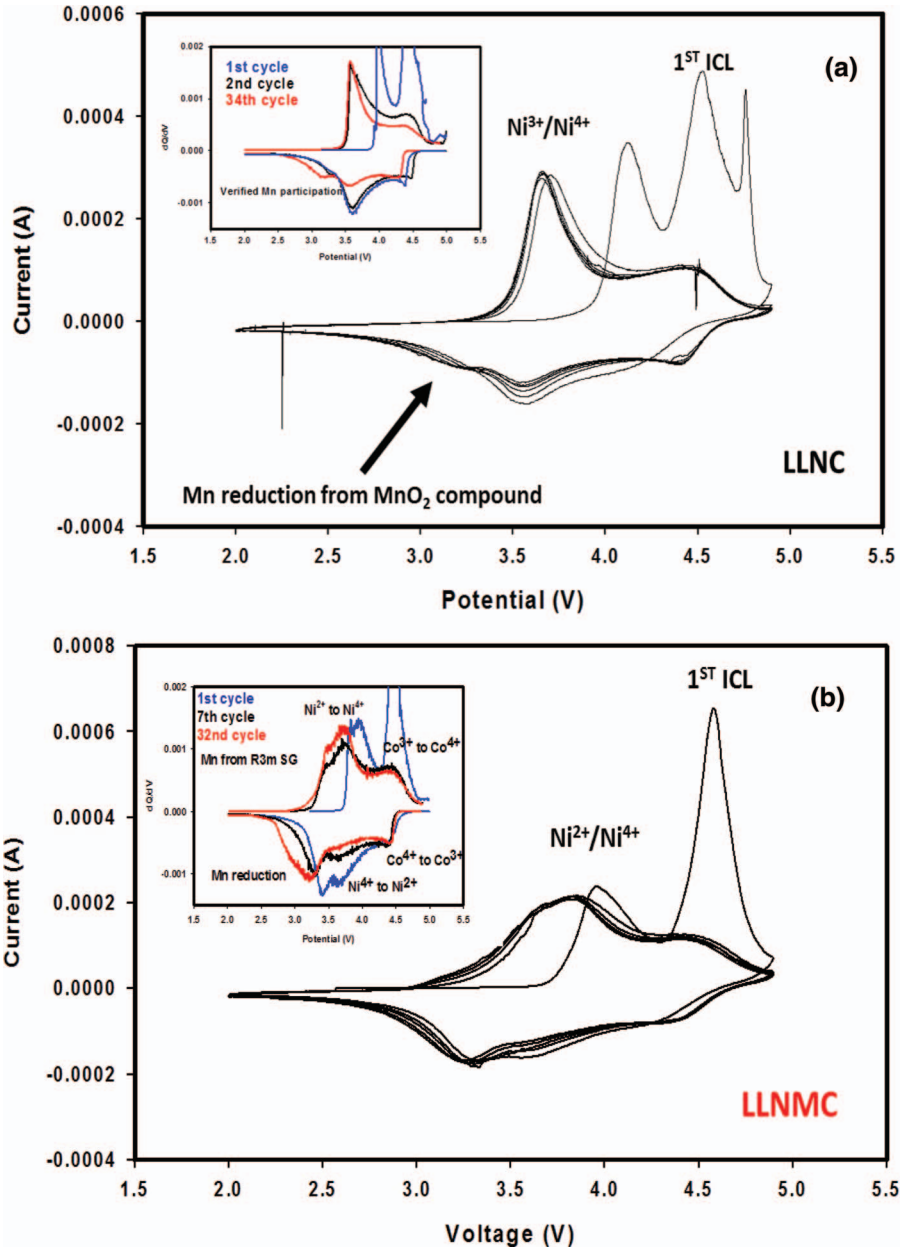

Figure 5. Cyclic Voltammetry behavior of a-) LLNC; and b-) LLNMC cathodes cycled between 2.0 and 4.9 V. The inset figure shows dQ/dV derivative plot of galvanostatically charged and discharged LLNC and LLNMC cell.

LLNMC is that, as mentioned in the previous section, Ni is not fully reduced to Ni^{2+} in the former. In LLNC, Ni is reduced and oxidized approximately between 3^+ and 4^+ valance states. The other piece of information from this figure is that the first charge plateau region between 4.3 and 4.9 V which is a direct indication of the amount of Li_2MnO_3 is almost the same in both LLNMC and LLNC. To investigate further whether the two compounds have similar amount of Li_2MnO_3 portion, we ran cyclic voltammetry (CV) sweeps of Li cells at room temperature with similar loadings. Figure 5a and 5b show the CV data for the first several cycles of LLNC and LLNMC, respectively. If one look carefully at the first irreversible capacity loss (ICL) peak at around 4.6 V, where the Li_2MnO_3 activation takes place, both materials have similar intensities. Moreover, in the first charging process for both LLNC and LLNMC cathodes, the oxidation peaks corresponding to Ni atoms shifted to lower potentials which is an indication of structural rearrangements after the first cycle.[13] Furthermore, the peaks assigned to Ni atoms have slightly different features for both materials during charging process. The Ni peak in LLNC has sharper oxidation peak while in LLNMC, it is broader. This is perhaps due to the fact that in LLNMC Ni^{2+} is oxidized to Ni^{4+} through multiple steps (Ni^{2+}–Ni^{3+}–Ni^{4+}) whereas in LLNC Ni^{2+} is oxidized to Ni^{3+} only. In addition, the peak intensities attributed to Ni oxidation (at around 3.7 V) is considerably different for the two materials with LLNC exhibiting higher intensities than LLNMC. This is expected since LLNC has a higher amount of Ni than LLNMC. As can be gleaned from Figure 5a, the slow growth of a peak between 3 and 3.5 V during the reduction process clearly indicated Mn participation from the MnO_2[31] produced from the activation of Li_2MnO_3. This peak continued to grow during further cycling as seen from the inset of Figure 5a that features dQ/dV plots of the galvanostatic cycling data for LLNC at room temperature. Similar Mn participation was observed for LLNMC which can be seen in the inset of Figure 5b.

Electrochemical cycling and rate capability data are displayed in Figures 6a and 6b for LLNC and LLNMC, respectively. They clearly demonstrate that LLNC has better rate capabilities than LLNMC. The C/20 rate discharge capacity for LLNMC did not change during sixty cycles in which many cycles were obtained at rates between C/5 and 2C. Likewise, for LLNC, the C/20 discharge capacity obtained after 50 cycles was around 165 mAh/g close to the initial discharge capacity shown in Figure 6a. For LLNMC, the discharge capacity at the C-rate,

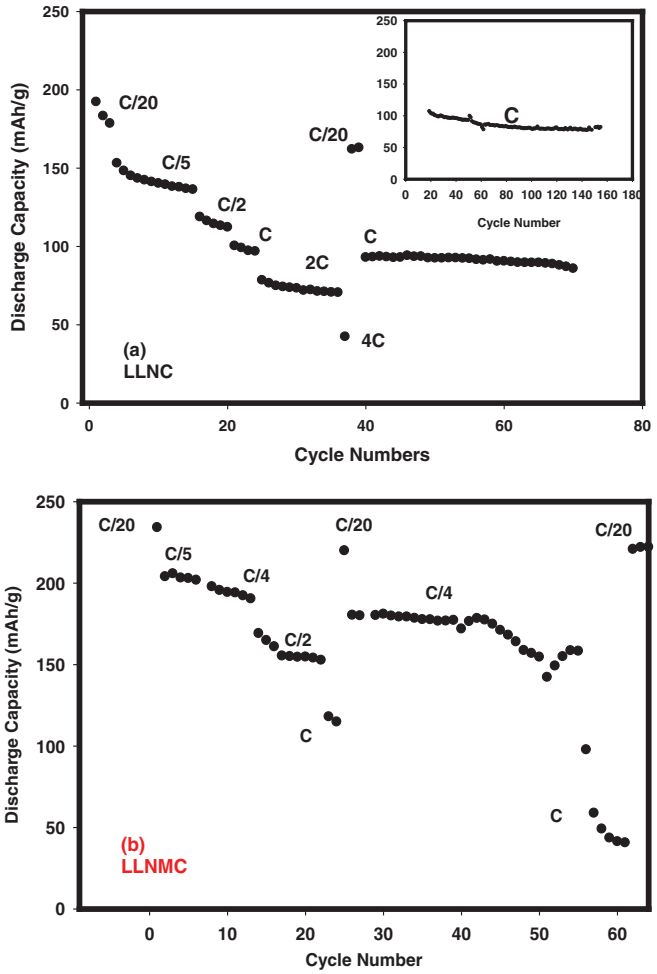

Figure 6. Cycling behavior of a-) LLNC and b-) LLNMC at different discharge rates between 2 and 4.9 V at room temperature. Charging rates were set at C/20. (1C = 280 mA/g).

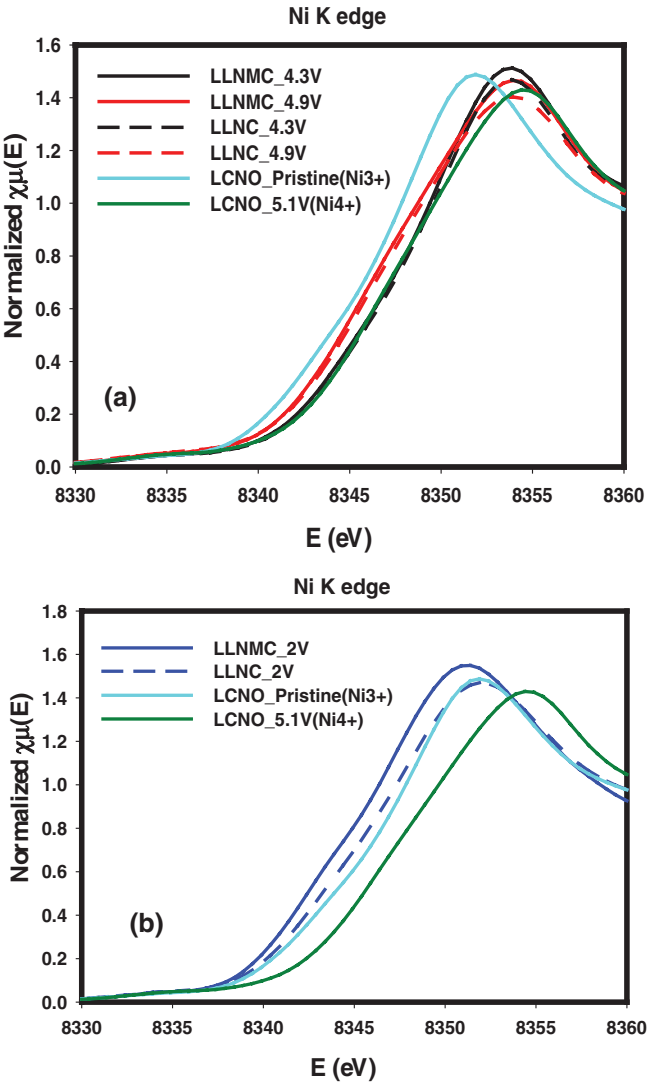

Figure 7. a-) Ni K-Edge XANES data of several samples including reference compounds with respect to their potentials in Li cells. b-) after the first discharge to 2 V.

measured after 20 low rate cycles, shown in Figure 6b, was about 120 mAh/g. The high rate capability of this material continued to decline with repeated cycling as indicated by a C-rate capacity close to 25 mAh/gram from the 56th to the 60th cycle. The data in Figure 6a show that LLNC capacity does not fade in the same manner at high rates. The high rate cycling data displayed in the inset in Figure 6a demonstrates very stable capacity for over 140 cycles at the C-rate for LLNC. As we explain below the improved cycling stability of LLNC can be attributed the absence of Mn in the $LiMO_2$ segment of this material and the mitigation of the layered to spinel conversion.

Additional structural information from XAS analysis during the first cycle.— X-ray absorption (XAS) is a useful tool to gain information on the local coordination environment of a specifically selected atom along with its valence state. The information gained from electrochemical data was complemented with XAS. Since Mn K-edge shift is not clear enough to distinguish the valence states due to its complex location in both the Li_2MnO_3 (C2/m SG) and $LiMO_2$ (R3m SG) layered segments where they have similar valance states,[29] we performed our first experiments at Ni K-edge whose redox couples transit between 2^+ and 4^+. The three points selected to investigate the Ni shifts were 4.3 V, 4.9 V and 2 V during the first cycle. The first cycle capacities of LLNC and LLNMC were similar to those shown in Figure 4. Both charging and discharging rates were set at C/20 in order to allow efficient Li extraction. We used $LiNi_{0.85}Co_{0.15}O_2$ as Ni^{3+} reference and it was charged to 5.1 V to obtain Ni^{4+} reference as reported by Balasubramanian et al.[16] XANES data of Ni K-edge are plotted in Figure 7a and 7b along with the reference compounds. Once the Li cell began to charge, the shift toward higher energy is observed (Figure 7a) due to the higher valance state of Ni in both cases. Contrary to some previous reports that claim Ni is being oxidized fully to 4^+ oxidation state in the lithium rich composite electrode materials, our experiments revealed that the valance state of the Ni ions is slightly below 4^+ at 4.9 V in both LLNC and LLNMC electrodes. Similar observations were reported elsewhere.[29,32] At the 4.3 V and 4.9 V charging points, both of the composite cathodes have similar Ni valence states. This is anticipated since Ni is in $LiMO_2$ segment of the composite where Ni is oxidized before the cell voltage reach 4.5 V as demonstrated in the CV data (see Figure 5). Nevertheless, at the first discharge end point of 2 V, Ni in LLNMC is reduced more compared to the Ni in LLNC as evidenced by higher XANES energy (eV) profile (see Figure 3a) for LLNC compared to LLNMC. We believe this less reduced state of Ni in LLNC is certainly responsible for its lower capacity (200 mAh/g) compared to LLNMC (240 mAh/g). From Figure 7b, one can deduce that Ni in LLNC shuttles between 3^+ and slightly less than 4^+. Traditional Fourier Transforms (FT) EXAFS analysis was applied to the Ni-K edge. Figure 8 displays this data for LLNC and LLNMC after one full cycle to 2 V. From this figure, one can tell that LLNMC has larger Ni-O bond length compared to LLNC.

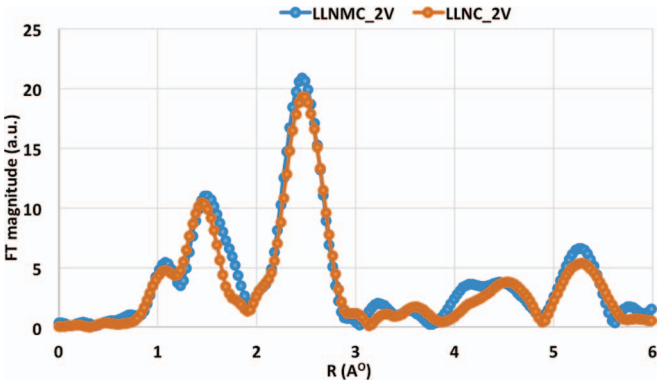

Figure 8. k3 weighted FT for the Ni absorber atom at Ni-K edge of both LLNC and LLNMC after the first discharge to 2 V.

This is because Ni is reduced more in LLNMC than in LLNC (see Figure 7b). Thus reducing the Ni atoms less in LLNC (Ni^{4+} to Ni^{3+}) than in LLNMC helps stabilize the former structure because it experiences less expansion and contraction during the redox process. On the contrary, in LLNMC Ni is being shuttled between Ni^{2+} (0.65A) and Ni^{4+} (0.48A) which produce larger structural stress in this material with repeated charge/discharge cycling. This larger ionic radius difference between Ni^{2+} and Ni^{4+} may trigger more cation mixing with Ni migrating to Li sites and ultimately causing layered to spinel structural transformation in LLNMC. On the other hand, Ni atoms in LLNC shuttle between Ni^{3+} (0.56A) and Ni^{4+} (0.48) which has less volume change during cycling and may inhibit structural transformation. The layer to spinel transformation behavior of the two materials is discussed in the next section.

Since we observed a major change in Ni-K edge at the first discharge end point (2 V), we also performed Mn-K edge experiments to support our observation from CV results for clear electrochemical participation of the MnO_2 produced from the activation of Li_2MnO_3. The two charge and discharge points selected to study Mn-K edge shifts were 4.9 V and 2 V. These data were compared to the as-synthesized materials. Figures 9 displays normalized XANES spectrum of the Mn-K edge of both compounds along with the spinel reference compound which has 3.5^+ valance state. From this spectrum, one can easily surmise that in both LLNC and LLNMC, the valence states are identical at 4.9 V during the first charge and after one full cycle ending at 2 V. The redox states for Mn at 4.9 V is believed to be higher

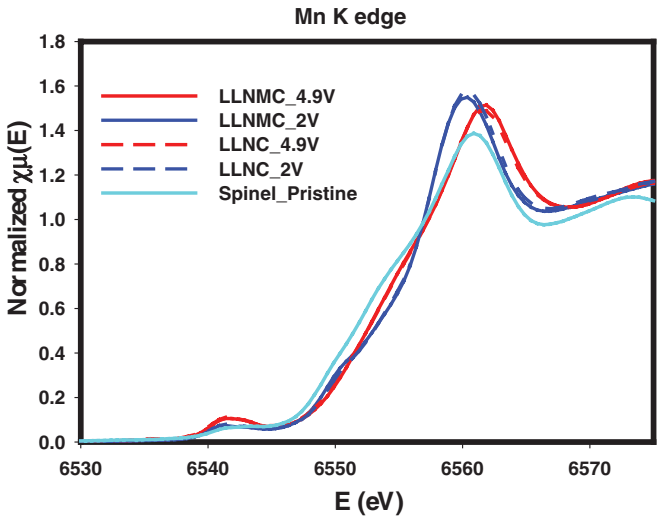

Figure 9. Normalized Mn-K edge XANES spectra of LLNC and LLNMC at room temperature at various potentials with respect to spinel reference.

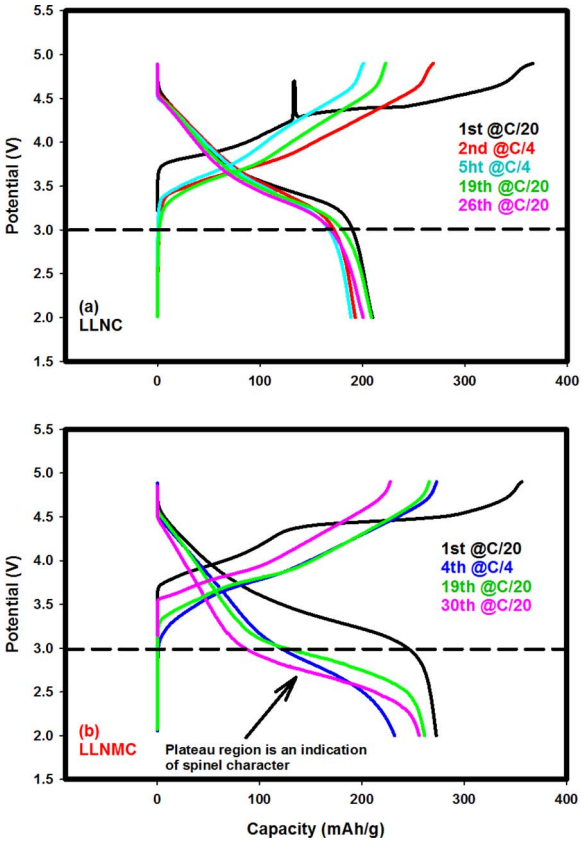

Figure 10. Charge-Discharge profiles of coin Li anode cells containing cathodes. a-) LLNC; b-) LLNMC. The cells were cycled at 50°C between 2 and 4.9 V.

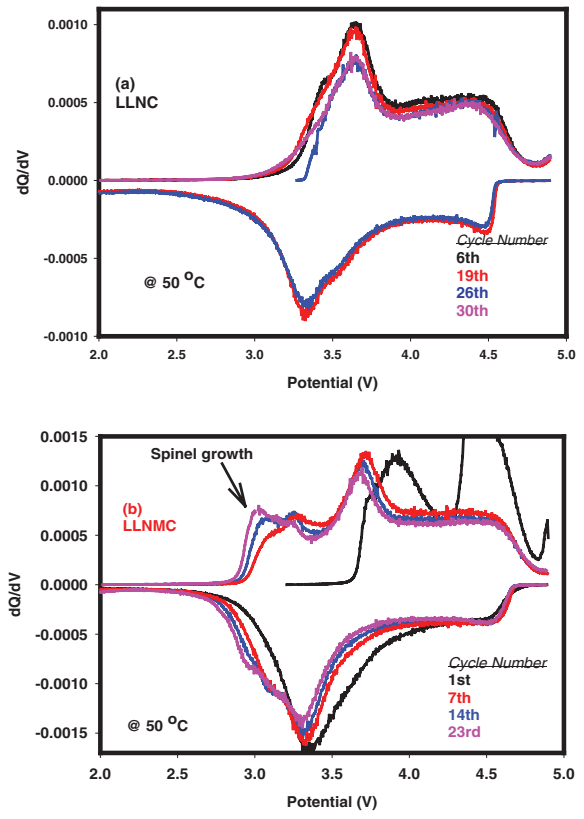

Figure 11. Derivative capacity (dQ/dV) plots of: a) LLNC b-) LLNMC at 50°C, between 2 and 4.9 V.

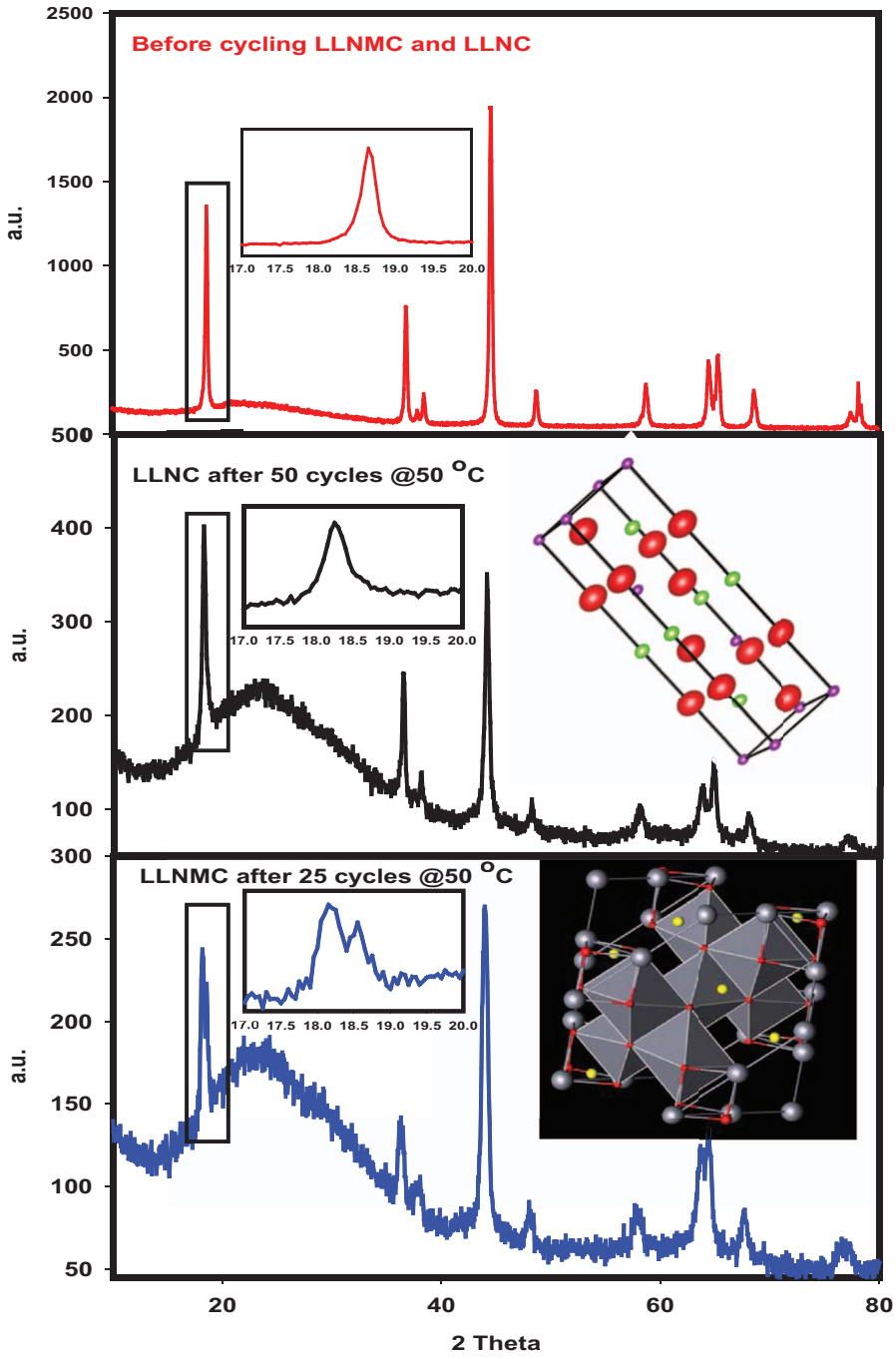

Figure 12. Ex situ XRD patterns before and after the 50°C cycles of LLNC and LLNMC compounds. The cycle numbers are indicated in the figure for each material. The LLNC and LLNMC have identical XRD patterns before cycling.

than 3.5^+ (closer to 4^+), and at 2 V not too lower than 3.5^+ as in the Mn spinel oxide. This notable similarity in Mn participation suggests i-) Mn from MnO_2 produced after the charge is participating in the redox reaction ii-) both Mn from the $LiMO_2$ and Li_2MnO_3 segments in $0.3Li_2MnO_3 0.7LiMn_{0.33}Ni_{0.33}Co_{0.33}O_2$ have similar redox behavior during the first charge and discharge. The question of which Mn participation triggers the layered to spinel conversion is well addressed with XAS data complemented by cell cycling data at both RT and at 50°C. This is discussed in the next section.

Layered to spinel structural transformation.— We were particularly interested in finding out if removal of Mn atoms from the $LiMO_2$ segment of the LLNC composite material mitigated the layered to spinel structural conversion. We characterized the cycling behavior of both the LLNC and LLNMC cathodes at 50°C. It is believed that at higher temperatures, the layered to spinel metal oxide structural conversion of the Li-rich composites is accelerated due to Mn^{2+} formation according to the disproportionation reaction, $Mn^{3+} \rightarrow Mn^{2+} + Mn^{4+}$.[2] The formation of Mn^{2+} apparently takes place through Jahn-Teller active Mn^{3+}[20] which is easier to decompose at higher temperatures.[9]

We studied the layered to spinel conversion of the two lithium rich materials through galvanostatic charging and discharging of coin cells at 50°C. In this experiment, each coin cell was weighed before and after the experiments to follow any electrolyte loss during the cycling. There was no weight change suggesting excellent seal integrity for the cells during the experiment. Figure 10a and 10b show the charge/discharge voltage-capacity profiles of LLNC and LLNMC electrodes, respectively, at 50°C. Each figure displays the cycle number and the applied rate. From these set of figures, it is clear that LLNC

has lower columbic efficiency than LLNMC at 50°C. While LLNC has similar discharge capacity at both RT (200 mAh/g) and 50°C (210 mAh/g), LLNMC possess higher discharge capacity (∼280 mAh/g) at the higher temperature than at RT (∼240 mAh/g). This is anticipated since Mn participation in redox reaction is triggered at high temperature as stated previously. It is, therefore, plausible to obtain lower columbic efficiency for LLNC which has less Mn than LLNMC. This further supports our conclusion that Mn atoms in LLNC are located in the Li_2MnO_3 rather than $LiMO_2$ portion of the compound.

It should be noted that the larger irreversible capacity of LLNMC would be desirable for anode such as silicon, or some new materials identified in the future, which exhibit significantly higher irreversible capacity than graphite. In the case of Si an excess of Si in the anode to absorb the Li might be desirable to construct a practical battery since the very high specific capacity of Si anode dictates the preparation of very thin anodes which often is difficult. In addition, for some applications an excess Li capacity on the anode as elemental Li is desirable for providing longer cycle life for the Li-ion battery. This can be accomplished with LLNMC or LLNC while it is not possible to do that with the traditional cathode materials without sacrificing significant energy density. Another advantage of LLNC is that it does not decompose during overcharge which the traditional NMC is prone to.

In Figure 10b for LLNMC, a clear voltage decay occurs with the voltage depressing to a plateau below 3 V. Several authors have attributed this behavior[2,14] to the layered to spinel conversion of the LLNMC. Interestingly, in Figure 10a, which depicts the cycling of LLNC, this behavior is inhibited. Furthermore, the differential capacity (dQ/dV) plots shown in Figure 11a and 11b for LLNC and LLNMC, respectively, demonstrates a clear spinel growth at ∼3 V during the oxidation half cycle for LLNMC (Figure 11b) which is absent in Figure 10a for LLNC. The peak at ∼3.3 V during discharge can be ascribed to the reduction of Mn from the layered MnO_2 produced after the activation of the Li_2MnO_3 segment of the composite structure. The absence of an oxidation peak (at ∼3 V) for Mn spinel phase in LLNC is another tell-tale indication that the layered to spinel structural conversion was mitigated in this composite cathode. The XRD profiles of post discharge samples of both electrode materials provided further support to this conclusion. Figure 12 displays the XRD patterns of the lithium rich electrodes before cycling and after 50 cycles for LLNC and 25 cycles for LLNMC, all at 50°C. The LLNC exhibits a robust structure by maintaining the symmetry of the (003) the peak even after 50 cycles at the high temperature. On the other hand, after just 25 cycles LLNMC reveals a clear split of the (003) peak suggesting that the layered to spinel structural conversion took place in this metal oxide as revealed from the charge-discharge cycling and dQ/dV profiles at 50°C. The peak splits and new peak growth appeared in the first (003) peak of LLNMC were previously attributed to the layered to spinel conversion feature by other groups.[21,33] The hexagonal crystals with R3m space group and spinel crystals with Fd3m space groups are presented in Figure 12 to visualize this structural conversion phenomenon.

Conclusions

We have synthesized and characterized a new lithium rich composite cathode material of the composition $0.3Li_2MnO_30.7LiNi_{0.5}Co_{0.5}O_2$. This material exhibited higher rate capability and structural stability during cycling than its previously known counterpart of the composition 0.3Li2MnO3.0.7$LiMn_{0.33}Ni_{0.33}Co_{0.33}O_2$. The removal of Mn from the $LiMO_2$ segment of the composite oxide structure has led to the mitigation of the layered to spinel conversion of the oxide. We demonstrated more than 50 cycles at 50°C for the $0.3Li_2MnO_30.7LiNi_{0.5}Co_{0.5}O_2$ cathode without any voltage depression or structural conversion. Its counterpart, $0.3Li_2MnO_30.7LiMn_{0.33}Ni_{0.33}Co_{0.33}O_2$, exhibited significant voltage depression and changes in X-ray diffraction pattern characteristic of the layered to spinel structural conversion just after 25 cycles at 50°C. The results obtained here indicates that the Mn present in the $LiMO_2$ segment of the composite oxide triggers the layered to spinel conversion in the Lithium rich composite oxides. The initial lower capacity of LLNC is attributed to the fact that the Ni ions present in the $LiMO_2$ segment has 3^+ oxidation state which limits its capacity. The XAS data confirm that the MnO_2 produced form the activation of Li_2MnO_3 in the initial charge participate in the redox reactions of the LLNC electrode although it does not appear to contribute to the layered to spinel structural transformation.

References

1. Z. Lu and J. R. Dahn, *Journal of The Electrochemical Society*, **149**, A815 (2002).
2. M. M. Thackeray, C. S. Johnson, J. T. Vaughey, N. Li, and S. A. Hackney, *Journal of Materials Chemistry*, **15**, 2257 (2005).
3. Z. Q. Deng and A. Manthiram, *The Journal of Physical Chemistry C*, **115**, 7097 (2011).
4. G. Singh, R. Thomas, A. Kumar, and R. S. Katiyar, *Journal of The Electrochemical Society*, **159**, A410 (2012).
5. K. Karthikeyan, K. W. Nam, E. Y. Hu, X. Q. Yang, and Y. S. Lee, *Bulletin of the Korean Chemical Society*, **34**, 1995 (2013).
6. Z. Li, N. A. Chernova, J. Feng, S. Upreti, F. Omenya, and M. S. Whittingham, *Journal of The Electrochemical Society*, **159**, A116 (2011).
7. F. Cheng, J. Chen, H. Zhou, and A. Manthiram, *Journal of The Electrochemical Society*, **160**, A1661 (2013).
8. G. Singh, R. Thomas, A. Kumar, R. S. Katiyar, and A. Manivannan, *Journal of The Electrochemical Society*, **159**, A470 (2012).
9. S. K. Martha, J. Nanda, Y. Kim, R. R. Unocic, S. Pannala, and N. J. Dudney, *Journal of Materials Chemistry A*, **1**, 5587 (2013).
10. F. Cheng, Y. Xin, J. Chen, L. Lu, X. Zhang, and H. Zhou, *Journal of Materials Chemistry A*, **1**, 5301 (2013).
11. Y. Zhao, W. Ren, R. Wu, Y. Yue, and Y. Sun, *J Solid State Electrochem*, **17**, 2259 (2013).
12. J. R. Croy, S. H. Kang, M. Balasubramanian, and M. M. Thackeray, *Electrochemistry Communications*, **13**, 1063 (2011).
13. S. H. Kang, P. Kempgens, S. Greenbaum, A. J. Kropf, K. Amine, and M. M. Thackeray, *Journal of Materials Chemistry*, **17**, 2069 (2007).
14. J. R. Croy, D. Kim, M. Balasubramanian, K. Gallagher, S.-H. Kang, and M. M. Thackeray, *Journal of The Electrochemical Society*, **159**, A781 (2012).
15. D. Im, J. Kim, J. Yoon, K.-S. Park, Y.-G. Ryu, S. S. Lee, D. J. Lee, and S.-G. Doo, *Electrochemical Society Meeting Abstracts*, **MA2010-01**, 630 (2010).
16. M. Balasubramanian, X. Sun, X. Q. Yang, and J. McBreen, *Journal of The Electrochemical Society*, **147**, 2903 (2000).
17. K. Momma and F. Izumi, *Journal of Applied Crystallography*, **44**, 1272 (2011).
18. M. Newville, *Journal of Synchrotron Radiation*, **8**, 322 (2001).
19. B. Ravel and M. Newville, *Journal of Synchrotron Radiation*, **12**, 537 (2005).
20. C. S. Johnson, N. Li, C. Lefief, J. T. Vaughey, and M. M. Thackeray, *Chemistry of Materials*, **20**, 6095 (2008).
21. F. Amalraj, M. Talianker, B. Markovsky, D. Sharon, L. Burlaka, G. Shafir, E. Zinigrad, O. Haik, D. Aurbach, J. Lampert, M. Schulz-Dobrick, and A. Garsuch, *Journal of The Electrochemical Society*, **160**, A324 (2013).
22. A. Ito, K. Shoda, Y. Sato, M. Hatano, H. Horie, and Y. Ohsawa, *Journal of Power Sources*, **196**, 4785 (2011).
23. M. M. Thackeray, S. H. Kang, C. S. Johnson, J. T. Vaughey, and S. A. Hackney, *Electrochemistry Communications*, **8**, 1531 (2006).
24. D. Kim, J. Gim, J. Lim, S. Park, and J. Kim, *Materials Research Bulletin*, **45**, 252 (2010).
25. N. Li, R. An, Y. Su, F. Wu, L. Bao, L. Chen, Y. Zheng, H. Shou, and S. Chen, *Journal of Materials Chemistry A*, **1**, 9760 (2013).
26. W. Liu, G. Fang, B. Xia, H. Sun, S. Kaneko, and D. Li, *RSC Advances*, **3**, 15630 (2013).
27. M. Y. Son, Y. J. Hong, S. H. Choi, and Y. C. Kang, *Electrochimica Acta*, **103**, 110 (2013).
28. M. Han, T. Sun, P. Y. Tan, X. Chen, O. K. Tan, and M. S. Tse, *RSC Advances* (2013).
29. A. Ito, Y. Sato, T. Sanada, M. Hatano, H. Horie, and Y. Ohsawa, *Journal of Power Sources*, **196**, 6828 (2011).
30. W.-S. Yoon, S. Iannopollo, C. P. Grey, D. Carlier, J. Gorman, J. Reed, and G. Ceder, *Electrochemical and Solid-State Letters*, **7**, A167 (2004).
31. H. Yu, H. Kim, Y. Wang, P. He, D. Asakura, Y. Nakamura, and H. Zhou, *Physical Chemistry Chemical Physics*, **14**, 6584 (2012).
32. J. R. Croy, M. Balasubramanian, D. Kim, S.-H. Kang, and M. M. Thackeray, *Chemistry of Materials*, **23**, 5415 (2011).
33. L. Xiao, Y. Zhao, Y. Yang, Y. Cao, X. Ai, and H. Yang, *Electrochimica Acta*, **54**, 545 (2008).